Acta Materialia 135 (2017) 77–87

Contents lists available at ScienceDirect

Acta Materialia

journal homepage: www.elsevier.com/locate/actamat

Full length article

Lattice strain evolution and load partitioning during creep of a Ni-based superalloy single crystal with rafted γ′ microstructure

James Coakley [a, b, *], Dong Ma [c], Matthew Frost [d], David Dye [e], David N. Seidman [a, f], David C. Dunand [a], Howard J. Stone [b]

[a] Northwestern University, Department of Materials Science and Engineering, Evanston, IL 60208-3108, USA
[b] Department of Materials Science and Metallurgy, University of Cambridge, Cambridge CB3 0FS, UK
[c] Oak Ridge National Laboratory, Chemical and Engineering Materials Division, Neutron Sciences Directorate, Oak Ridge, TN 37831, USA
[d] Oak Ridge National Laboratory, Instrument and Source Division, Oak Ridge, TN 37831, USA
[e] Department of Materials, Imperial College, South Kensington, London SW7 2AZ, England, UK
[f] Northwestern University Center for Atom-Probe Tomography (NUCAPT), 2220 Campus Drive, Evanston, IL, 60208, USA

ARTICLE INFO

Article history:
Received 20 March 2017
Received in revised form
9 June 2017
Accepted 9 June 2017
Available online 12 June 2017

Keywords:
Superalloys
Precipitation
Neutron diffraction
Creep
Directional coarsening

ABSTRACT

In-situ neutron diffraction measurements were performed on monocrystalline samples of the Ni-based superalloy CMSX-4 during N-type γ′ raft formation under the tensile creep conditions of 1150 °C/100 MPa, and subsequently on a rafted sample under the low temperature/high stress creep conditions of 715 °C/825 MPa. During 1150 °C/100 MPa creep, the γ′ volume fraction decreased from ~70% to ~50%, the lattice parameter misfit was partly relieved, and the load was transferred from the creeping γ matrix to the γ′ precipitates. On cooling back to room temperature, a fine distribution of γ′ precipitates formed in the γ channels, and these precipitates were present in the 715 °C/825 MPa creep regime. Under low temperature/high stress creep, the alloy with rafted γ′ microstructure exhibited superior creep strength to the cuboidal γ′ microstructure produced following a standard heat-treatment. A lengthy creep incubation period was observed, believed to be associated with {111}⟨110⟩ dislocations hindering propagation of {111}⟨112⟩ dislocations. Following the creep incubation period, extensive macroscopic creep strain accumulated during primary creep as the γ phase yielded. Finally, the diffraction data suggest a loss of precipitate/matrix coherency in the (0k0) interfaces as creep strain accumulated.
© 2017 Acta Materialia Inc. Published by Elsevier Ltd. All rights reserved.

1. Introduction

Ni-based superalloys have been the material of choice over the last 75 years for high temperature applications requiring a combination of excellent strength and creep resistance, as well as corrosion and oxidation resistance [1,2]. Ni-based superalloys are strengthened by coherent (L12) precipitates (γ′) with a base stoichiometry of Ni3(Al,Ti) embedded within a (fcc) Ni-matrix (γ) [3]. Rafting, also termed stress coarsening, occurs in superalloys exposed to both elevated stresses and temperatures (i.e. under creep conditions), and the orientation of the rafts of aligned coalesced γ′ particles is dependent on both the direction of the applied load and the lattice parameter misfit of the alloy $\delta = 2[a_{\gamma'} - a_{\gamma}]/[a_{\gamma'} + a_{\gamma}]$, where $a_{\gamma'}$ and a_{γ} are the lattice parameters of the γ′ and γ phases, respectively [4]. Modern Ni-based superalloys used for single crystal turbine blades typically have a negative lattice parameter misfit at creep and coarsening temperatures, and particle coalescence thus occurs normal to the tensile loading direction to form a plate-like structure on the transverse face (N-type raft) [4,5]. Under compressive load, such negative lattice parameter misfitting alloys form rods aligned parallel to the loading direction (P-type raft) [4,5].

Co-based superalloys, that also possess γ/γ′ precipitate strengthened microstructures, are currently under rapid development as a potential successor to the now mature Ni-based superalloys [6–23]. In contrast to the Ni-based superalloys, the Co-based superalloys developed to date typically have a positive lattice parameter misfit, and it is therefore expected that the γ′ rafts of a crept Co-superalloy would be orientated normal to a compressive load (N-type raft), and parallel to a tensile load (P-type raft) [24]. The difference in direction of coalescence of the strengthening γ′

* Corresponding author. Northwestern University, Department of Materials Science and Engineering, Evanston, IL 60208-3108, USA.
E-mail address: james.coakley@northwestern.edu (J. Coakley).

http://dx.doi.org/10.1016/j.actamat.2017.06.021
1359-6454/© 2017 Acta Materialia Inc. Published by Elsevier Ltd. All rights reserved.

precipitates between Ni- and Co-based superalloys directly influence their mechanical properties.

High temperature/low stress rafting creep has been studied with particular focus on the role of dislocations, through finite element modelling [4,25,26], through examination of crept samples by transmission electron microscopy (TEM) [4,5,25–31], and through room temperature diffraction [26]. By their very nature, these studies have been performed under temperature and stress conditions that are very different to those that generate the rafted γ' microstructure. The evolution of lattice parameter misfit in Ni-based superalloys during thermal exposures and under specific creep conditions have been studied by *in-situ* diffraction [32–38]. However, these studies have not correlated the lattice parameter misfits measured with direct observations of the rafting behaviour.

Given the differences in raft orientations of the Co- and Ni-based superalloy systems, studies relating γ' raft type and direction to mechanical properties of both superalloy systems are timely. The current work firstly presents *in-situ* diffraction measurements focusing on the formation of the N-type rafts that grow during tensile creep at 1150 °C/100 MPa in the Ni-based superalloy CMSX-4 [27]. The decrease in γ' volume fraction at elevated temperature is determined, along with the effect of creep primarily occurring in the γ channels.

Secondly, *in-situ* diffraction measurements of CMSX-4 with a rafted γ' microstructure were performed during low temperature/high stress creep at 715 °C/825 MPa to study the load partitioning between rafted γ' precipitates and the γ matrix. The creep strength and load-partitioning are compared to previously published *in-situ* diffraction measurements during creep of CMSX-4 with a cuboidal microstructure. In general, N-type rafts are considered to be a degradation of the microstructure, with a deterioration of mechanical properties including: (i) high temperature/low stress non-isothermal creep strength [39]; (ii) thermomechanical fatigue resistance [40]; and (iii) ambient and elevated temperature yield strength [41]. However, it is noted in this work that a pre-rafted microstructure results in a creep hardening effect, and the rafted γ' microstructure is superior to the cuboidal γ' microstructure under low-intermediate temperature/high stress creep conditions. A lengthy creep incubation period is observed in the pre-rafted microstructure with little to no strain accumulation at 650–715 °C/825 MPa prior to primary creep. This is in contrast to the cuboidal microstructure [38]. Following the creep incubation period, the γ phase yielded and the diffraction data suggests that the precipitates lose coherency with the matrix in the (0k0) interfaces as creep strain accumulated.

2. Experimental procedures

2.1. Material processing

Single crystal bars of the Ni-based superalloy CMSX-4 were provided by Rolls-Royce plc., Derby, following their standard heat-treatment process: (i) a proprietary solution heat-treatment to dissolve the γ' phase and reduce the levels of elemental segregation followed by a fast cool; (ii) a primary aging treatment of 1140 °C/2 h; (iii) a secondary aging treatment of 870 °C/16 h. Secondary electron SEM images were recorded with a Hitachi SU8030 cold-field emission scanning electron microscope operated at 2 kV with a 3–6 mm working distance, after electrolytically etching the γ phase with an aqueous solution of 2.5 vol% phosphoric acid at 2.5 V dc for ~1 s.

2.2. Creep and neutron scattering

Cylindrical tensile-creep bars of the single crystal Ni-based superalloy with 12.7 mm gauge diameter and 40 mm gauge length were machined from the heat-treated rods. The samples were tested on VULCAN [42], the time-of-flight (TOF) neutron engineering diffractometer at the spallation neutron source (SNS), Oak Ridge National Laboratory (ORNL), Tennessee. Samples were mounted such that the tensile stress was applied along the nominal [100] direction. The irradiated length of each sample was 7 mm, centred at the middle of the specimen gauge length, and the experimental procedure was similar to that previously described elsewhere [38]. The loading axis was horizontal and the rig was positioned to give the longitudinal (h00) diffraction peaks in one detector and the transverse (0k0) diffraction peaks in the other.

Diffraction measurements were performed on two samples to study *in-situ*: (i) the evolution of lattice strain in the γ and the γ' phases and the lattice parameter misfit during N-type γ' raft formation; and (ii) to compare the internal load transfer between phases during low temperature/high stress creep conditions of an N-type rafted γ' microstructure to previously published data for a cuboidal γ' microstructure [38].

A sample was mounted to collect diffraction data of:

1. The initial heat-treated condition, at room temperature and zero stress, with a beam frequency of 20 Hz in high intensity mode and collecting data for 15 min;
2. During creep with *in-situ* neutron diffraction at 1150 °C/100 MPa, with a beam frequency of 20 Hz in high intensity mode. The diffracted beam was collected in the detectors continuously during the 14 h creep test, and the data were subsequently chopped into 20 min segments. This creep condition is known to induce rafting [27].

As heat was applied to the sample from an induction coil with the sample grips chilled by internal water cooling, a strong thermal gradient was present across the sample. An extensometer was not used during the *in-situ* rafting measurement, therefore the creep test was repeated three times *ex-situ* with a 12 mm extensometer. Thermocouples were mounted along all samples, and the temperature difference across the 12 mm extensometer mounted at the sample center was determined to be 5 to 10 °C. The thermal gradient across the central 7 mm irradiated length was lower than these bounds (as the irradiated length lay within the extensometer), and this length was therefore approximately isothermal.

A sample that had been rafted ex-situ at 1150 °C/100 MPa for 10 h was used to collect diffraction data of:

1. The γ' rafted condition at room temperature and zero stress, with a beam frequency of 60 Hz in high resolution mode and collecting data for 20 min;
2. During creep with *in-situ* neutron diffraction at 715 °C/825 MPa, with a beam frequency of 60 Hz in high resolution mode. The diffracted beam was collected in the detectors continuously during the ~18 h creep test, and the data were subsequently chopped into 20 min segments;
3. Following the creep test, at room temperature and zero stress, with a 60 Hz beam frequency in high resolution mode and collecting data for 5 min.

An *in-situ* diffraction creep measurement was also performed on a rafted γ' microstructure during a two-step creep experiment at 650 °C/825 MPa/12 h followed by creep at 725 °C/825 MPa. The results are discussed briefly in this paper, and compared to the 650 °C/825 MPa *in-situ* diffraction creep measurement for CMSX-4 with a cuboidal γ' microstructure [38].

3. Results

3.1. Initial material characterisation

The microstructure of the single crystal Ni-based superalloy, Fig. 1a, possesses a near-unimodal distribution of submicron cuboidal γ' precipitates within a γ matrix. A low number density of fine nanoscale γ' precipitates were also present in the γ channels. The total areal fraction of the γ' precipitates determined via binary thresholding and pixel counting of SEM images was ~73 ± 3%, in agreement with the volume fraction stated in the literature (~70% [43]). The mean width ($\overline{w}$) of the submicron γ' precipitates was $\overline{w}$ = 510±40 nm with standard deviation calculated from traced areas using square-equivalence ($\overline{w} = \overline{\text{area}}^{1/2}$).

3.2. 1150 °C/100 MPa rafting creep of cuboidal microstructure: macroscopic creep curves and microscopy

After a short creep incubation period of around 0.2 h, the Ni-based superalloy samples (i) - (iii) accumulated about 0.3%–0.5% primary creep strain over the first 1 h–2 h of tensile creep at 1150 °C/100 MPa, followed by quasi-steady-state creep, Fig. 1b. The samples accumulated 0.7%–1% total creep strain over the full 10 h creep test.

From the SEM images acquired from the single crystal Ni-based superalloy following tensile rafting creep at 1150 °C/100 MPa/10 h (~0.7% accumulated creep strain), it is apparent that the creep conditions induced a coarse plate-like (or more specifically, an amoeba-like) γ' microstructure with their planes aligned perpendicular to the applied load, Fig. 1c and d. The areal fraction of these rafted precipitates was ~52 ± 3% from the (0k0) planes, transverse to the loading direction, using the pixel counting method of representative micrographs described previously. Referring to the (0k0) plane, Fig. 1c, the rafts were approximately 0.3–0.5 μm in width in the axial loading direction, and 1–20 μm in length transverse to the loading direction. Given the similarity of the width of the rafts to the width of the original cuboidal microstructure, it is clear that, under the applied tensile stress and temperature, the resultant coarsening was directional and perpendicular to the loading direction. It is interesting to note in the CMSX-4 micrographs that the γ matrix channels between the rafted γ' precipitates were filled with nanoscale γ' precipitates of two further size distributions with diameters ~25–75 nm and ~10 nm, respectively, as shown in Fig. 2. It is likely these nanoscale γ' precipitates form on cooling from 1150 °C to room temperature, as the phase field broadens. Finally, the SEM micrograph shown in Fig. 2 reveals that the large γ' rafts are composed of a two phase nanostructure, possibly γ precipitating within γ' during cooling. However, confirmation of this would require a thorough and advanced TEM-based study.

3.3. 715 °C/825 MPa low temperature/high stress creep of rafted microstructure: macroscopic creep curves

An *in-situ* diffraction creep test was first performed on the rafted microstructure at 650 °C/825 MPa, labelled (ii) in Fig. 3. This creep condition was selected to allow for direct comparison with the *in-situ* diffraction measurements of the cuboidal γ' microstructure measured at 650 °C/825 MPa (Fig. 3, curve (iv)) [38]. This low temperature creep condition is known to not induce rafting in the time-scales presented (under 24 h) [38]. The cuboidal γ' microstructure accumulated ~6.6% macroscopic creep strain over the first

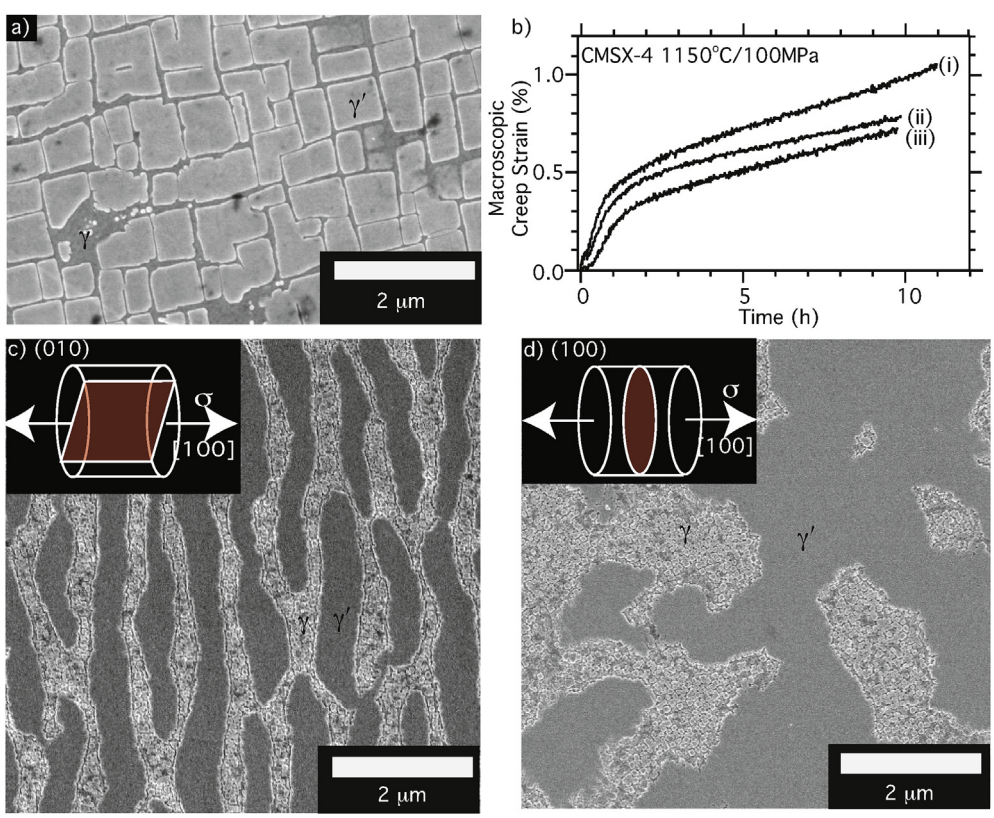

Fig. 1. Representative secondary emission SEM images of etched cross-sections of the single crystal Ni-based superalloy (CMSX-4) showing the γ–γ' microstructure of a) the initial heat-treated condition, c) the (010) longitudinal plane following tensile creep and raft formation at 1150 °C/100 MPa, d) the corresponding (100) transverse plane. b) Macroscopic creep curves of three samples (i) - (iii) that induce rafting; the post-creep SEM shown in (c–d) is from the sample used for the creep test designated (ii).

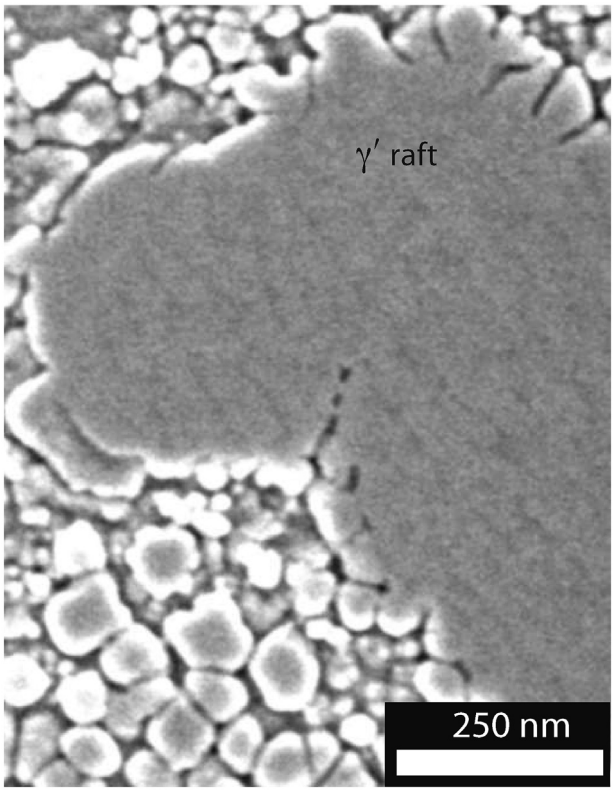

Fig. 2. (100) high magnification secondary emission SEM image of CMSX-4 crept in tension at 1150 °C/100 MPa/10 h showing the γ′ raft and fine γ′ precipitates in the etched γ matrix. A nanostructure within the γ′ raft is evident.

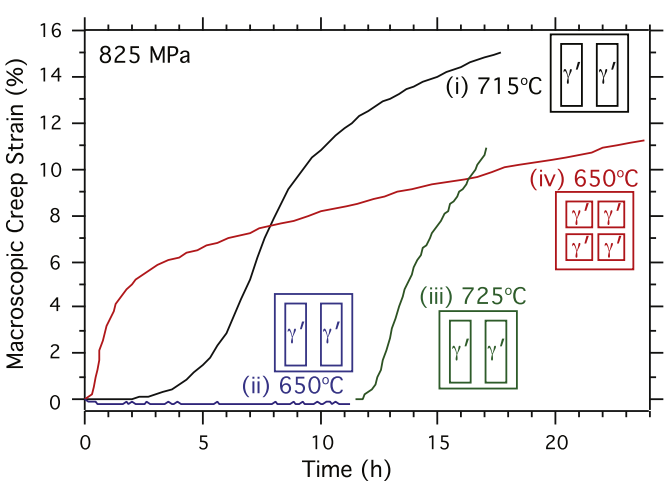

Fig. 3. i - iii) Macroscopic creep curves of CMSX-4 with a rafted γ′ microstructure (see Fig. 1c–d) crept (i) at 715 °C/825 MPa, (ii) initially at 650 °C/825 MPa and then the temperature was increased to give creep at (iii) 725 °C/825 MPa. (iv) Macroscopic creep curve of CMSX-4 with a cuboidal γ′ microstructure (see Fig. 1a) at 650 °C/825 MPa[38].

5 h, and 8.1% strain over 10 h. In comparison, the rafted microstructure remained in what is presumably a creep incubation period for the 12 h creep test, accumulating no plastic strain. Thus, the γ′ rafted microstructure is superior under the creep conditions and times studied. The creep temperature was then progressively increased to induce primary creep, and at 725 °C a very rapid creep rate was observed (Fig. 3, curve (iii)). From this initial test, it was possible to optimise the creep conditions for an *in-situ* diffraction study, and a second creep test was performed on a rafted γ′ microstructure at 715 °C/825 MPa, labelled (i) in Fig. 3. After an incubation period of ~2 h, a large amount of creep strain was accumulated over the subsequent 10 h of primary creep, reaching ~12.5% creep strain. The strain rate decreased over the final 6 h of the creep test, accumulating a further ~2.5% creep strain in this time. Both samples failed by shear, away from the sample center, presumably due to the thermal gradient across the samples during plastic deformation.

3.4. Neutron diffraction peak fitting

Prior to creep, when the precipitates are cuboidal, and during the *in-situ* diffraction rafting creep measurement at 1150 °C/100 MPa, the {300} γ′ peaks were symmetric in shape. At room temperature following rafting creep, when the γ′ precipitates were rafted and plate-like with finer γ′ also present in the γ channels (Fig. 1c–d), the (300) γ′ peak was located at a higher d-spacing value compared to the initial measurement. This (300) peak, corresponding to the rafted microstructure, was asymmetric with a pronounced tail towards lower d-spacings. This was mirrored by the (030) γ′ peak, which exhibited a stronger tail at higher d-spacings to the maximum peak intensity following rafting creep. These {300} peak shapes were also observed during the *in-situ* diffraction primary creep measurement at 715 °C/825 MPa, Fig. 4a and b.

Peak fitting routines were developed and applied to the diffraction data, based on those available in the literature [16,21,22,33–35,37,38,44–46]. The γ′ {300} peaks prior to creep and during *in-situ* rafting creep (1150 °C/100 MPa) were symmetric, and fitted well with a single pseudo-Voigt function by an iterative least squares error minimisation procedure to the diffraction data. Following the rafting creep treatment, the subsequent γ′ {300} peaks at room-temperature and *in-situ* low temperature/high stress creep conditions (715 °C/825 MPa) were fitted with two pseudo-Voigt functions to account for the lattice parameters of the two γ′ populations present. For comparison, they were also fitted with the single pseudo-Voigt function.

The (200) and (020) γ+γ′ doublet peaks appeared to be symmetric prior to rafting creep [38], indicating that the constrained γ and γ′ lattice parameter misfit was initially very low and the individual peaks were closely overlaid. Following rafting creep at 1150 °C/100 MPa, the (200) γ+γ′ doublet peak was broad, with maximum intensity to the right of the doublet, Fig. 4c. The higher intensity peak of the doublet is associated with the γ′ phase, given the alloy is ~70% volume fraction γ′ at room temperature and the larger average bound coherent scattering length of atoms in the γ′ phase compared to that of the γ [33]. Thus, the alloy is of positive lattice parameter misfit in the (200) after rafting creep at 1150 °C/100 MPa. The opposite is evident in the (020) peak, with the high intensity peak to the left of the doublet, Fig. 4d, indicating negative lattice parameter misfit in the (020) following rafting creep at 1150 °C/100 MPa.

As the lattice parameter misfit is initially low, the {200} peaks of the Ni-based superalloy prior to rafting creep at 1150 °C/100 MPa and during the *in-situ* rafting creep diffraction measurements were fitted by pseudo-Voigt doublets by constraining $d^{\gamma'}_{\{200\}} = (3/2) \times d^{\gamma'}_{(300)}$, in order to fit the {200} γ peak position. The pseudo-Voigt peak shape and width were defined as being equal for both the γ and γ′ phases in order to reduce the number of fitting parameters, consistent with other studies [38,45]. Following the rafting procedure, the γ and γ′ {200} peaks at room temperature and during 715 °C/825 MPa *in-situ* creep were more separated.

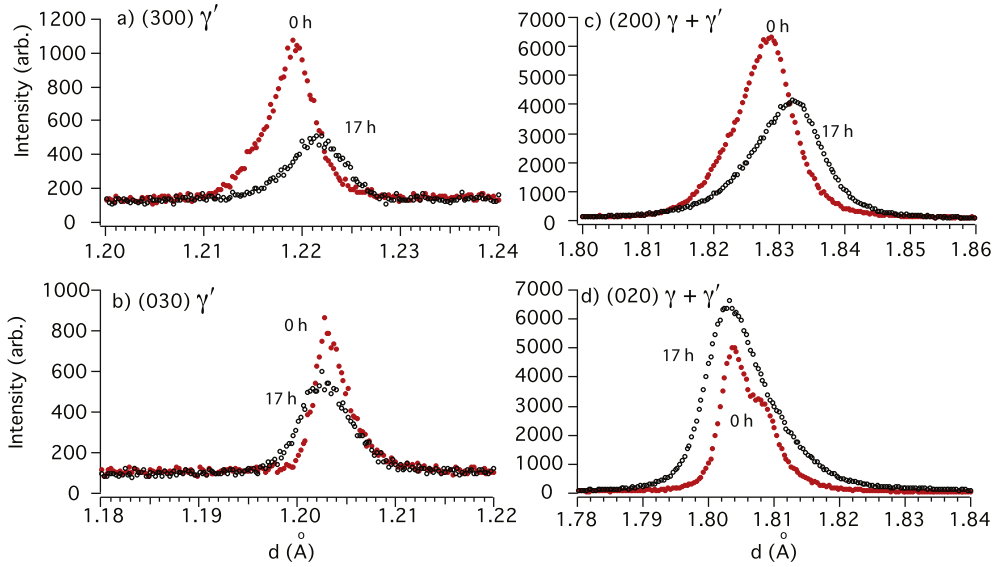

Fig. 4. *In-situ* neutron diffraction data of selected reflections from CMSX-4 with a rafted γ' microstructure at 715 °C/825 MPa at the beginning of the creep test (0 h) and towards the end of the creep test (17 h).

These peaks were fitted with the same doublet $\gamma+\gamma'$ peak fitting routine, but without the $d^{\gamma'}_{\{200\}} = (3/2) \times d^{\gamma'}_{(300)}$ constraint. Good agreement was found for $d^{\gamma'}_{\{200\}}$ and $(3/2) \times d^{\gamma'}_{(300)}$. A triple peak function was also fitted to the {200} diffraction peaks, in order to separate the contributions from the two different size distributions of γ' particles to the diffraction data. This required additional constraints to be introduced to the peak fitting routine, and it was found that the residual error of the overall peak fit to the data was larger than that of the doublet peak function. Thus, the doublet $\gamma+\gamma'$ peak fitting routine was applied to the data, and the slight error introduced by combining the two γ' diffraction peaks into a single peak is acknowledged. Examples of the peak fits are illustrated in Fig. 5.

3.5. Lattice parameter evolution at 1150 °C/100 MPa

The (h00) γ and γ' lattice parameter data at room temperature and zero stress before and after rafting creep at 1150 °C/100 MPa are shown in Fig. 6i, region (a) and region (c) of the graph, respectively. The evolution of the lattice parameters during rafting creep at 1150 °C/100 MPa is shown in region (b). The corresponding (0k0) lattice parameter data are shown in Fig. 6ii. To aid the discussion and interpretation, the lattice parameter evolution of each phase during creep is plotted in terms of elastic lattice strain changes that occur in each phase during creep alone, $\varepsilon_c = (a_x - a_{x,0})/a_{x,0}$ where $a_{x,0}$ is the lattice parameter at the start of the creep test (1150 °C/100 MPa), Fig. 7. Finally, the data is replotted in terms of lattice parameter misfit δ, Fig. 8.

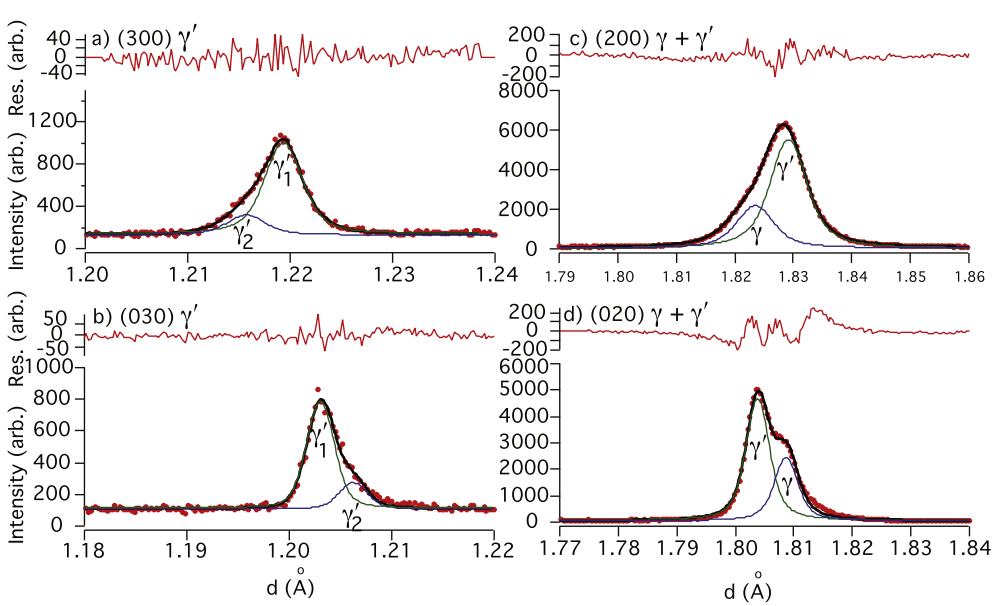

Fig. 5. Pseudo-Voigt doublet fits to the longitudinal (a, c) and transverse (b, d) banks diffraction data showing the (a, b) (300) and (030) γ' and (c, d) (200) and (020) $\gamma+\gamma'$, respectively. The *in-situ* diffraction data shown are for the first 20 min of creep at 715 °C/825 MPa of CMSX-4 with a rafted microstructure. (a, b) Doublet fits that account for the two γ' lattice parameters observed, and (c, d) doublet fits for the γ' and γ peak contributions.

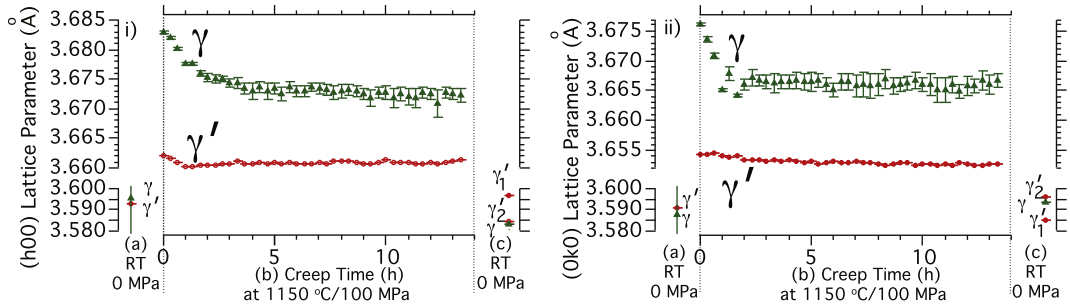

Fig. 6. i) (h00) and (ii) (0k0) γ and γ' lattice parameters of CMSX-4 with initial cuboidal γ' microstructure at room temperature and zero stress (a) prior to creep and (c) post-creep, and (b) evolution of the lattice parameters during creep at 1150 °C/100 MPa. The two lattice parameters of γ' following cooling are distinguished by the same notation as Fig. 5, where the subscript 1 always denotes the higher intensity peak. The error bars presented are associated with the error in the peak fits.

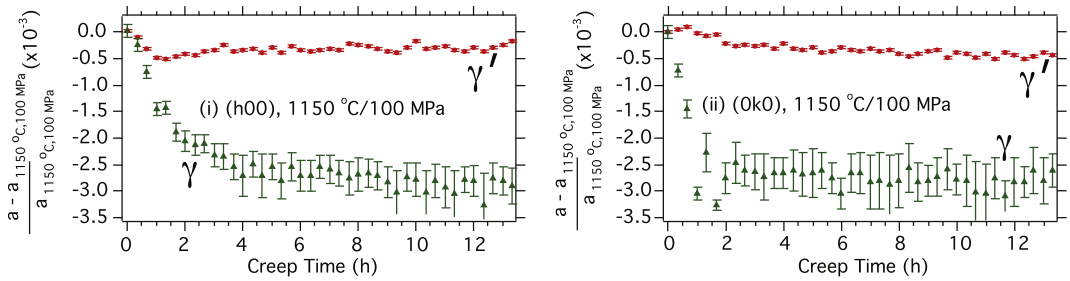

Fig. 7. Evolution of the elastic lattice strain in the γ and γ' phases of CMSX-4 with initial cuboidal γ' microstructure that occurs during tensile creep at 1150 °C/100 MPa in the (i) (h00) and (ii) (0k0) lattice planes. The error bars presented were calculated from the lattice parameter errors.

3.6. Lattice parameter evolution at 715 °C/825 MPa

The peak fitting results of the 715 °C/825 MPa low temperature/high stress creep diffraction data are presented in Figs. 9–11, in the same manner as previously described for the rafting creep data at 1150 °C/100 MPa, but with $a_{x,0}$ defined in this case as the lattice parameter of phase x at the start of the low temperature/high stress creep test (715 °C/825 MPa).

4. Discussion

4.1. Creep-induced microstructural evolution and observation by in-situ diffraction

The evolution of deformation mechanisms and microstructural parameters that are stress, temperature, and time dependent inherently complicates our understanding of creep. Fig. 12 is a schematic representation of how certain creep-induced phenomena would be observed in a negative lattice parameter misfit superalloy when measuring the γ and γ' phase lattice parameters *in-situ* by neutron diffraction. A uniform three-dimensional loss of coherency of the γ' phase within the γ matrix would be observed equally in the detectors measuring (h00) and (0k0) lattice spacings as a decrease in the γ' lattice parameter and an increase in the γ lattice parameter, Fig. 12a and b. This occurs as atomic registry across the interface plane is lost, and the γ' lattice parameter approaches its equilibrium unconstrained value. Similarly, the γ lattice parameter will increase towards its equilibrium value as a result of the loss of constraint by the γ' phase. A significant repartitioning of elements at temperature would also be observed equally in both detectors, with the schematic example illustrating partitioning of elements with large atomic radii from the γ' to the γ and assuming precipitate volume fraction is constant. This would be observed as a decrease of the γ' lattice parameter and an increase of the γ lattice parameter, Fig. 12a and b. It has previously been illustrated that the lattice parameter misfit becomes increasingly negative with temperature for CMSX-4 [47], suggesting that such repartitioning may indeed occur.

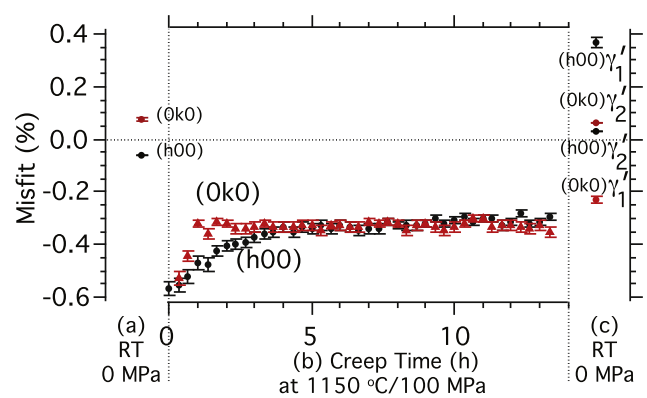

Fig. 8. (h00) and (0k0) lattice parameter misfit of CMSX-4 with initial cuboidal microstructure at room temperature and zero stress (a) prior to creep and (c) post-creep, and (b) the evolution of the (h00) and (0k0) lattice parameter misfit during rafting creep at 1150 °C/100 MPa. The two lattice parameter misfit values following cooling are distinguished by the same notation as for Fig. 5, where the subscript 1 always denotes the higher intensity γ' peak. Error bars of 5% are presented.

If load transfer occurs to the γ' phase under yielding of the γ phase, this would be observed as an increase in the γ' lattice parameter and a decrease in the γ lattice parameter in the (h00), with an associated Poisson effect observed in the (0k0), Fig. 12c and d.

During creep of a superalloy single crystal, the tensile axis rotates towards the slip direction. Given that the [100] direction is the least stiff direction [21,44,48], the rotation is towards a stiffer direction and would be observed as a decrease of lattice parameter

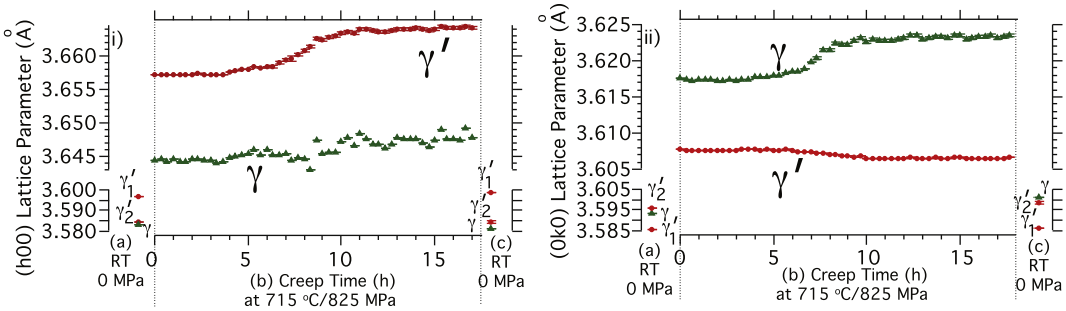

Fig. 9. i) (h00) and (ii) (0k0) γ and γ' lattice parameters of CMSX-4 with initial rafted γ' microstructure at room temperature and zero stress (a) prior to creep and (c) post-creep, and (b) evolution of the lattice parameters during creep at 715 °C/825 MPa. The two lattice parameters of γ' following cooling are distinguished by the same notation as Fig. 5, where the subscript 1 always denotes the higher intensity peak. The error bars presented are associated with the error in the peak fits.

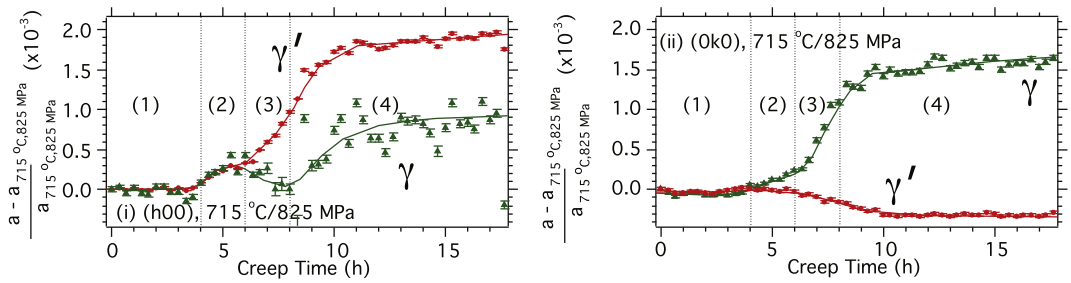

Fig. 10. Evolution of the elastic lattice strain of CMSX-4 with initial rafted γ' microstructure that occurs during tensile creep alone $\varepsilon_c = (a - a_{715^\circ C,825\ MPa})/a_{715^\circ C,825\ MPa}$ of γ and γ' at 715 °C/825 MPa in the (i) (h00) and (ii) (0k0) lattice planes. Trend lines have been added as guides to the eye and the graph is segmented to aid discussion. The error bars presented were calculated from the lattice parameter errors.

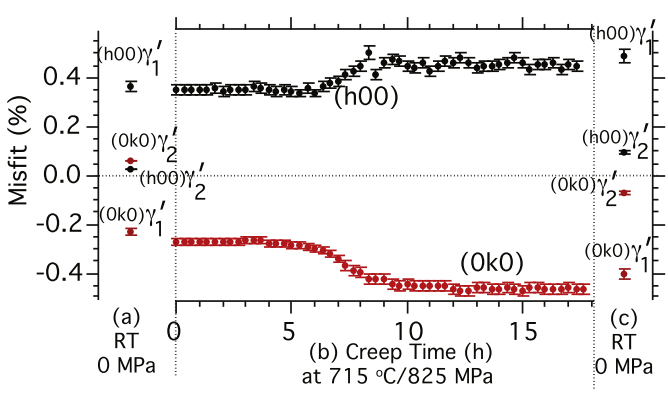

Fig. 11. (h00) and (0k0) lattice parameter misfit of a rafted microstructure at room temperature and zero stress prior to and post primary creep at 715 °C/825 MPa, (a) and (c) respectively, and the evolution of the (h00) and (0k0) lattice parameters during primacy creep (b). The two lattice parameter misfit values following cooling are distinguished by the same notation as for Fig. 5, where the subscript 1 always denotes the higher intensity γ' peak. Error bars of 5% are presented.

value in both phases in the (h00) during creep at a constant stress σ, as $\sigma = \varepsilon E$, Fig. 12e. This would be accompanied by a Poisson effect in the (0k0), Fig. 12f.

On rapidly heating to the creep temperature, the $\gamma+\gamma'$ is in a non-equilibrium mix, and equilibrium will be achieved according to the Lever Rule, by (i) dissolution of γ' and (ii) shifting of phase compositions towards equilibrium at the creep temperature. Considering first the effect of precipitate dissolution on the stress distribution between the two phases, as the constrained elastic moduli of the γ ($E\gamma$) and the γ' ($E_{\gamma'}$) phases are approximately equal [33,49], a stress redistribution will not occur between the precipitate and matrix due to a change in the precipitate volume fraction. Now considering the change in phase compositions towards equilibrium in the Ni-Al binary phase diagram [50,51], the $\gamma/\gamma+\gamma'$ phase boundary has a relatively shallow slope against temperature compared to the $\gamma+\gamma'/\gamma'$ phase boundary which is near vertical. For a vertical $\gamma+\gamma'/\gamma'$ phase boundary, the γ' equilibrium composition will be approximately constant with temperature, and only a change in the γ composition will occur. Therefore this shift towards phase equilibria at temperature accompanied by dissolution of the γ' would be observed equally in both detectors as a decrease in the γ lattice parameter while that of the γ' would remain unchanged, Fig. 12g and h. For the case of Ni-based superalloys, a slight shift in the γ' lattice parameter may be expected if the $\gamma+\gamma'/\gamma'$ phase boundary is less steep than that of Ni-Al.

A decrease in sample area, *i.e.* an increase in true stress, would be observed as an increase of lattice parameter value in both phases in the (h00) during creep, Fig. 12i, with a Poisson effect observed in the (0k0), Fig. 12j.

Work hardening of the γ phase during creep deformation would be observed as an increase of the γ lattice parameter and a decrease of the γ' lattice parameter in the (h00), with an associated Poisson effect in the transverse direction, Fig. 12k and l. The comparison of the experimental data to the schematic presented is necessary in order to correctly correlate the measured lattice spacing evolution to microstructural evolution.

4.2. 1150 °C/100 MPa rafting creep of cuboidal γ' microstructure

In the first ~2 h of creep at 1150 °C/100 MPa, there is a release of ~2.0–2.5 mε in the γ phase in both the (h00) and (0k0), Fig. 7. There is a much smaller release of ~0.2–0.5 mε in the γ' over the same time. Referring to the schematic in Fig. 12g and h and previous discussion, it is clear in the first 2 h of creep that the lattice parameter evolution measured is dominated by dissolution of γ' as

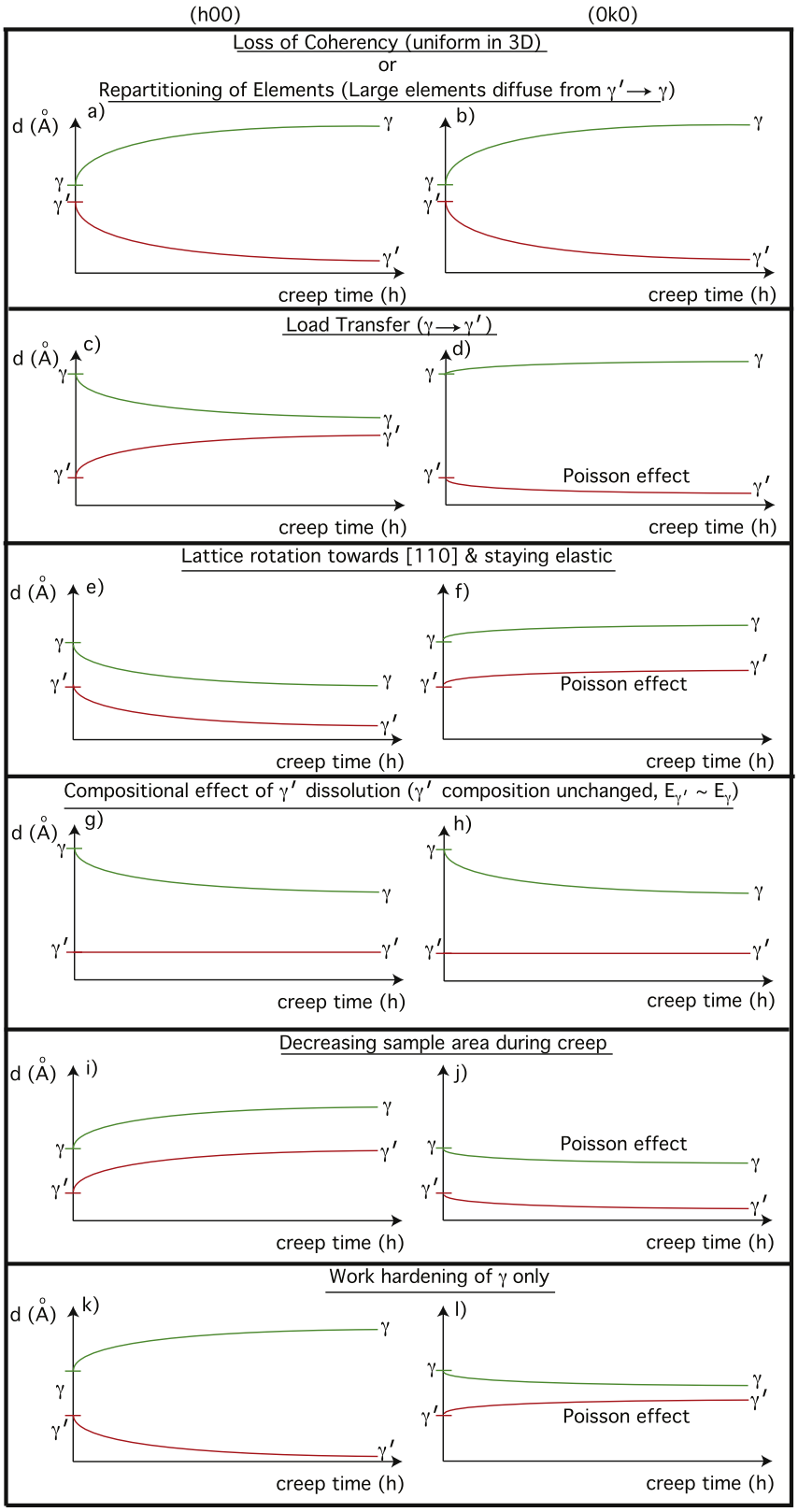

Fig. 12. Schematic plot of the lattice spacing evolution in both the (h00) and (0k0) of the γ and γ' phases during tensile creep along the nominal [h00] direction for a negative misfit alloy that would be observed as a result of various microstructural evolutions that may occur during creep, specifically: (a–b) if the γ' particles lose coherency with the γ matrix, or if there is diffusion of elements with large atomic radii from γ' to γ under constant precipitate volume fraction; (c–d) If the γ matrix yields and load is transferred to the γ' phase; (e–f) If there is lattice rotation towards the stiffer [110] direction; (g–h) If dissolution of γ' occurs during creep conditions, with no change in the γ' composition and both phases possessing similar elastic moduli; (i–j) If the sample area decreases during creep; (k–l) If there is work hardening of the γ phase alone.

the alloy approaches phase equilibrium at 1150 °C, observed as a large decrease in the γ lattice strains and a relatively small change in the γ' lattice strains in both planes, Fig. 7. The dissolution of γ' phase at elevated temperature was also apparent from the evolution of the γ and γ' diffraction peak intensities ($I\gamma$ and $I\gamma'$, respectively), determined by the {200} peak fitting routine. Initially at 1150 °C, the ratio of $I_{\gamma'}/(I_{\gamma'}+I_{\gamma}) \sim 0.7$, noted as being approximately equal to the precipitate volume fraction determined by SEM. This ratio decreased to ~0.6 after ~1.5 h of creep, and ~0.5 after ~4 h of creep, after which the ratio remained close to constant. It was previously noted that the volume fraction of γ' rafts was ~0.5 (50%) following creep at 1150 °C/100 MPa.

Over the subsequent 10 h of creep the lattice strain response is less dramatic. The data suggest that there is a small amount of load transfer from the γ to the γ' as the γ phase yields (Fig. 12c and d), apparent as a slight increase in the (h00) γ' lattice strain accompanied by a decrease in the (h00) γ and (0k0) γ' lattice strains (Fig. 7). This is consistent with the general consensus that, under high-temperature low-stress creep regimes the plastic deformation is confined to the γ channels [52].

Fig. 8 presents the data in terms of lattice parameter misfit. At room temperature before creep, the lattice parameter misfit is close to 0%, and ~−0.6% at the onset of rafting creep, due to the difference in thermal expansion coefficients between phases. Within 1 h the lattice parameter misfit in the (0k0) lattice plane is halved to ~−0.3%, and the same lattice parameter misfit is reached after ~4 h in the (h00) lattice plane. The decrease in magnitude of the lattice parameter misfit value is a result of the large change in the γ lattice parameter that occurs due to the change in the γ composition and γ' phase dissolution required to achieve phase equilibrium at 1150 °C.

It was noted earlier that the {300} peak shapes were initially quite symmetric at room temperature, and symmetric during the 1150 °C/100 MPa creep test, after which they were asymmetric on cooling to room temperature, and asymmetric during the subsequent 715 °C/825 MPa creep test. The tail is to the left (lower d-spacing) of the (300) peak, and to the right (higher d-spacing) of the (030), Fig. 4a and b. On cooling from 1150 °C following creep, the residual strain induced from the creep process is seen as a shift of the γ' peak to higher d-spacing values in the (300), and lower d-spacing values in the (030), relative to the initial room temperature measurement. The lower intensity γ' {300} peak that appears on cooling from 1150 °C, producing the overall peak asymmetry, is associated with nucleation of a second size distribution of γ'. This was observed in the SEM as fine γ' in the γ matrix channels, Fig. 1c and d. The difference in mean γ' lattice parameter value of each size distribution is associated with a difference in composition and presumably also a difference in coherency with the matrix as well as any interphase stresses.

4.3. 715 °C/825 MPa low temperature/high stress creep of rafted γ' microstructure

There is an initial incubation period of ~4 h where the lattice strains ε_c of both phases (Fig. 10 region (1)) and macroscopic creep strain (Fig. 3, curve i) are essentially zero, for the 715 °C/825 MPa low temperature/high stress creep test. High temperature/low stress creep is associated with {111}⟨110⟩ dislocation slip of the γ phase, while low-intermediate temperature/high stress creep is associated with {111}⟨112⟩ slip of both phases [53]. The incubation period is therefore related to generation of the required dislocations for slip to occur. More specifically, it is expected that the same dislocation mechanisms are active during primary creep of a rafted γ' microstructure, as for a cuboidal γ' microstructure, therefore the incubation period is associated with nucleation of {111}⟨112⟩ dislocations. Both nucleation and slip of these dislocations will be hindered by the pre-existing {111}⟨110⟩ dislocations in the γ phase, resulting in a lengthy creep incubation period. The rafted γ' sample was still in a creep incubation period after 12 h of creep at 650 °C/825 MPa with zero macroscopic strain accumulation, Fig. 3ii. After the 12 h test at 650 °C/825 MPa, the temperature was increased. From the lengthy creep incubation period and superior macroscopic creep strength, one can conclude that the pre-existing dislocations have strengthened the alloy under low temperature/high stress creep conditions, and that the combination of pre-existing dislocations and rafted γ' microstructure with fine γ' precipitates in the channel provides superior creep strength compared to the initial heat-treated alloy.

Following the creep incubation period, the lattice strain in both phases increased in the (h00) between 4 and 6 h of creep time, Fig. 10 region (2). This timeframe corresponded to rapid macroscopic strain accumulation during primary creep (Fig. 3 curve (i)), and therefore the decreasing sample area may have contributed to the observed lattice strains during the creep test (Fig. 12i). The transverse data do not show the typical Poisson effect associated with a decreasing sample area, but exhibit a lattice strain response that is consistent with yielding of the γ phase and load transfer to the γ', Fig. 12d of the schematic. The yielding of γ is also observed in region (3) of Fig. 10i, particularly in the (h00) where load is transferred from the γ to the γ'. At the onset of region (4) in the (h00), Fig. 10i, following the yielding of γ there is an increase in lattice strains of both phases, which is believed to be indicative of a continuous reduction in the sample area contributing to the diffraction data. Finally, it is noted that the difference in the (0k0) lattice strains between the phases towards the end of the creep test is too large to be associated with a Poisson effect alone, Fig. 10ii. Furthermore the (h00) and (0k0) γ data do not show a Poisson response in region (4) of the lattice strain data. Therefore, the divergence of the γ and γ' lattice spacing can be interpreted as a loss of coherency in the (0k0), Fig. 9ii. From the large length of the γ' rafts, a loss of coherency may indeed be expected in the (0k0). The loss of coherency between precipitate and matrix observed in the (0k0) data is observed as an increasingly negative lattice parameter misfit in the (0k0) data, Fig. 11.

Some similar trends in microstrain evolution are observed for the cuboidal γ' microstructure crept at 900 °C/460 MPa and crept at 650 °C/825 MPa [38], and the rafted microstructure crept at 715 °C/825 MPa in this work. The lattice strain response in Fig. 10 region (4), resembles that of the lattice strain data crept at 900 °C/460 MPa. The authors of the previous work concluded that the γ initially yields during creep [38], in agreement with the current work. The previous authors suggested that a large load transfer from γ to γ' in the (0k0) results in an increase in the γ (0k0) lattice parameter and a decrease in the γ (h00) lattice parameter. We note that the sample following 900 °C/460 MPa creep possessed a microstructure typical of early stage rafting, thus the interpretation presented in this work may apply to the previously published data: that the γ' loses coherency with the γ matrix in the (0k0). Some similarities are noted between the lattice strain responses to creep of a cuboidal γ' microstructure at 650 °C/825 MPa [38] and regions (1)–(3) of the 715 °C/825 MPa creep test with a rafted γ' microstructure performed in the present study. In both experiments, the (0k0) γ and γ' lattice strains were initially equal, after which the γ' lattice strain decreased and the γ increased. In the (h00), a decrease in the γ lattice strain, Fig. 10 region (3), was also common to both experiments. However, in the case of the 650 °C/825 MPa data [38], the γ' lattice strain did not increase, and the previous authors hypothesised that this must be due to a recovery mechanism. The data and interpretation of the current work are clearer, with evident load transfer to the γ' on yielding of the γ.

In summary, there is a long creep incubation period during creep of CMSX-4 with rafted γ' microstructure at 715 °C/825 MPa. This is associated with pre-existing {111}⟨110⟩ dislocations hindering the {111}⟨112⟩ dislocations required for creep under low temperature/high stress conditions. The creep incubation period is followed by rapid macroscopic strain accumulation during primary creep, and it appears that the decreasing sample area, and the concomitant increase in stress, is seen in the lattice strain evolution of each phase. The γ phase yields over a period of a few hours with load transfer to the γ'. Finally, the data suggest that there is a loss of coherency of the γ' precipitates with the γ matrix in the (0k0).

5. Summary & conclusions

In-situ neutron diffraction measurements have been performed on CMSX-4 during raft formation at 1150 °C/100 MPa, and during subsequent low temperature/high stress creep conditions of a sample with a rafted γ' microstructure.

During 1150 °C/100 MPa creep, the measured lattice strains and SEM observations reveal a rapid loss in γ' volume fraction from ~70% to ~50%. In this time period the lattice parameter misfit is partially relieved. Slight load transfer from γ to γ' is observed as creep proceeds.

On cooling back to room temperature from 1150 °C, a fine distribution of γ' precipitates nucleate and grow in the γ channels. These fine precipitates are present in the subsequent low temperature/high stress creep test of 715 °C/825 MPa. Under the creep conditions studied, the alloy with a rafted γ' microstructure exhibits superior creep strength to the cuboidal γ' microstructure following a standard heat-treatment.

A lengthy creep incubation period prior to primary creep is observed at 715 °C/825 MPa, suggested to be a consequence of the {111}⟨110⟩ dislocations present from the previous rafting creep regime (at 1150 °C/100 MPa) hindering subsequent generation and slip of {111}⟨112⟩ dislocations.

Primary creep is observed as an initial yielding of the γ phase following the creep incubation period. The diffraction data indicate that the γ' precipitates lose coherency with the γ matrix in the (0k0) during the creep test.

Acknowledgements

The authors acknowledge the contribution of Dr. Neil Jones of Rolls-Royce plc., Derby, UK, for providing samples. This work was performed under the following financial assistance award 70NANB14H012 from U.S. Department of Commerce, National Institute of Standards and Technology as part of the Center for Hierarchical Materials Design (ChiMad). JC acknowledges support from the European Union Seventh Framework Programme under the Marie Curie grant agreement No. 628643, and DD acknowledges support under EPSRC grants EP/M005607/1 and EP/L001748/1. The neutron scattering study at ORNLs Spallation Neutron Source was sponsored by the Scientific User Facilities Division, Office of Basic Energy Sciences, US Department of Energy. This work made use of the EPIC facility of the NUANCE Center at Northwestern University, which has received support from the Soft and Hybrid Nanotechnology Experimental (SHyNE) Resource (NSF NNCI-1542205); the MRSEC program (NSF DMR-1121262) at the Materials Research Center; the International Institute for Nanotechnology (IIN); the Keck Foundation; and the State of Illinois, through the IIN.

References

[1] R.C. Reed, The Superallloys: Fundamentals and Applications, Cambridge University Press, Cambridge, 2006.
[2] C.T. Sims, High-Temperature Materials for Aerospace and Industrial Power, Wiley, New York, 1987.
[3] E. Nembach, G. Neite, Precipitation hardening of superalloys by ordered γ'-particles, Prog. Mater. Sci. 29 (1985) 177–319.
[4] F.R.N. Nabarro, Rafting in superalloys, Metall. Mater. Trans. A 27 (3) (1996) 513–530.
[5] J.K. Tien, R.P. Gamble, Effects of stress coarsening on coherent particle strengthening, Metall. Trans. 3 (8) (1972) 2157–2162.
[6] J. Sato, T. Omori, K. Oikawa, I. Ohnuma, R. Kainuma, K. Ishida, Cobalt-base high-temperature alloys, Science 312 (5770) (2006) 90–91.
[7] A. Bauer, S. Neumeier, F. Pyczak, R.F. Singer, M. Göken, Creep properties of different γ'-strengthened Co-base superalloys, Mater. Sci. Eng. A 550 (2012) 333–341.
[8] A. Bauer, S. Neumeier, F. Pyczak, M. Göken, Creep strength and microstructure of polycrystalline gamma-prime-strengthened cobalt-base superalloys, in: Superalloys 2012: 12th International Symposium on Superalloys, 2012, pp. 695–703.
[9] F. Xue, H.J. Zhou, Q.Y. Shi, X.H. Chen, H. Chang, M.L. Wang, Q. Feng, Creep behavior in a γ' strengthened Co-Al-W-Ta-Ti single-crystal alloy at 1000°C, Scr. Mater 97 (2015) 37–40.
[10] F. Xue, H.J. Zhou, Q. Feng, Improved high-temperature microstructural stability and creep property of novel Co-base single-crystal alloys containing Ta and Ti, J. O. M. 66 (12) (2014) 2486–2494.
[11] F. Xue, H.J. Zhou, X.F. Ding, M.L. Wang, Q. Feng, Improved high temperature γ' stability of Co-Al-W-base alloys containing Ti and Ta, Mater. Lett. 112 (2013) 215–218.
[12] K. Shinagawa, T. Omori, K. Oikawa, R. Kainuma, K. Ishida, Ductility enhancement by boron addition in Co-Al-W high-temperature alloys, Scr. Mater. 61 (2009) 612–615.
[13] M.S. Titus, A. Suzuki, T.M. Pollock, Creep and directional coarsening in single crystals of new γ-γ' cobalt-base alloys, Scr. Mater. 66 (2012) 574–577.
[14] K. Tanaka, M. Ooshima, N. Tsuno, A. Sato, H. Inui, Creep deformation of single crystals of new Co-Al-W-based alloys with fcc/L12 two-phase microstructures, Philos. Mag. 92 (32) (2012) 4011–4027.
[15] M.S. Titus, Y.M. Eggeler, A. Suzuki, T.M. Pollock, Creep-induced planar defects in L12-containing Co- and CoNi-base single-crystal superalloys, Acta Mater. 82 (2015) 530–539.
[16] H.Y. Yan, V.A. Vorontsov, J. Coakley, N.G. Jones, H.J. Stone, D. Dye, Quaternary alloying effects and the prospects for a new generation of Co-base superalloys, in: Superalloys 2012: 12th International Symposium on Superalloys, 2012, pp. 705–714.
[17] L. Klein, M.S. Killian, S. Virtanen, The effect of nickel and silicon addition on some oxidation properties of novel Co-based high temperature alloys, Corros. Sci. 69 (2013) 43–49.
[18] M. Knop, P. Mulvey, F. Ismail, A. Radecka, K.M. Rahman, T.C. Lindley, B.A. Shollock, M.C. Hardy, M.P. Moody, T.L. Martin, P.A.J. Bagot, D. Dye, A new polycrystalline Co-Ni superalloy, J. O. M. 66 (12) (2014) 2495–2501.
[19] S.K. Makineni, B. Nithin, K. Chattopadhyay, A new tungsten-free γ-γ' Co-Al-Mo-Nb-based superalloy, Scr. Mater. 98 (2015) 36–39.
[20] S.K. Makineni, B. Nithin, K Chattopadhyay, Synthesis of a new tungsten-free γ-γ' cobalt-based superalloy by tuning alloying additions, Acta Mater. 85 (2015) 85–94.
[21] H.Y. Yan, J. Coakley, V.A. Vorontsov, N.G. Jones, H.J. Stone, D. Dye, Alloying and the micromechanics of Co-Al-W-X quaternary alloys, Mater. Sci. Eng. A 613 (2014) 201–208.
[22] F. Pyczak, A. Bauer, M. Göken, U. Lorenz, S. Neumeier, M. Oehring, J. Paul, N. Schell, A. Schreyer, A. Stark, F. Symanzik, The effect of tungsten content on the properties of L12-hardened Co-Al-W alloys, J. Alloys Compd. 635 (2015) 110–115.
[23] P.J. Bocchini, E.A. Lass, K.W. Moon, M.E. Williams, C.E. Campbell, U.R. Kattner, D.C. Dunand, D.N. Seidman, Atom-probe tomographic study of γ/γ' interfaces and compositions in an aged Co-Al-W superalloy, Scr. Mater. 68 (8) (2013) 563–566.
[24] H. Mughrabi, The importance of sign and magnitude of γ/γ' lattice misfit in superalloys-with special reference to the new γ'-hardened cobalt-base superalloys, Acta Mater. 81 (2014) 21–29.
[25] T.M. Pollock, A.S. Argon, Directional coarsening in nickel-base single crystals with high volume fractions of coherent precipitates, Acta Metall. Mater. 42 (6) (1994) 1859–1874.
[26] H. Biermann, B. vonGrossmann, T. Schneider, H. Feng, H. Mughrabi, Investigation of the γ/γ' morphology and internal stresses in a monocrystalline turbine blade after service: determination of the local thermal and mechanical loads, in: Superalloys 1996: 8th International Symposium on Superalloys, 1996, pp. 201–210.
[27] R.C. Reed, D.C. Cox, M.A. Rist, C.M.F. Rae, Creep of CMSX-4 superalloy single crystals: effects of rafting at high temperature, Acta Mater. 41 (12) (1999) 3367–3381.
[28] M. Kamaraj, Rafting in single crystal nickel-base superalloys - an overview, Sadhana 28 (1–2) (2003) 115–128.
[29] J. Lapin, M. Gebura, T. Pelachova, O. Bajana, Microstructure degradation of nickel base single crystal superalloy CMSX-4, Metal (2009) 304–310.
[30] A. Epishin, T. Link, M. Nazmy, M. Staubli, H. Klingelhöffer, G. Nolze, Microstructural degradation of CMSX-4: kinetics and effect on mechanical properties, in: Superalloys 2008: 11th International Symposium on Superalloys,

2008, pp. 725–731.
[31] N. Matan, D.C. Cox, C.M.F. Rae, R.C. Reed, On the kinetics of rafting in CMSX-4 superalloy single crystals, Acta Mater. 47 (7) (1999) 2031–2045.
[32] Y. Lu, S. Ma, B.S. Majumdar, Elastic microstrains during tension and creep of superalloys: results from in situ neutron diffraction, in: Superalloys 2008: 11th International Symposium on Superalloys, 2008, pp. 553–562.
[33] D. Dye, J. Coakley, V.A. Vorontsov, H.J. Stone, R.B. Rogge, Elastic moduli and load partitioning in a single-crystal nickel superalloy, Scr. Mater. 61 (2) (2009) 109–112.
[34] G. Bruno, B. Schönfeld, G. Kostorz, Lattice misfit in CMSX-4-like nickel-base superalloys and its temperature dependence, Z. Met. 94 (2003) 12–18.
[35] H.C. Pinto, G. Bruno, Formation and relaxation of coherency strain in the nickel-base superalloy SC16, J. Synchrotr. Rad. 10 (2003) 148–153.
[36] G. Bruno, H.C. Pinto, The kinetics of the γ' phase and its strain in the nickel-base superalloy SC16 studied by in-situ neutron and synchrotron radiation diffraction, in: Superalloys 2004: 10th International Symposium on Superalloys, 2004, pp. 837–848.
[37] G. Bruno, G. Schumacher, H.C. Pinto, C. Schulze, Measurement of the lattice misfit of the nickel-base superalloy SC16 by high-energy synchrotron radiation, Metall. Mater. Trans. A 34 (2003) 193–197.
[38] J. Coakley, R.C. Reed, J.L.W. Warwick, K.M. Rahman, D. Dye, Lattice strain evolution during creep in single-crystal superalloys, Acta Mater. 60 (2012) 2729–2738.
[39] R. Giraud, J. Cormier, Z. Hervier, D. Bertheau, K. Harris, J. Wahl, X. Milhet, J. Mendez, A. Organista, Effect of prior microstructure degradation on the high temperature/low stress non-isothermal creep behaviour of CMSX-4 Ni-based superalloy, in: Superalloys 2008: 11th International Symposium on Superalloys, 2008, pp. 265–274.
[40] M.M. Kirka, K.A. Brindley, R.W. Neu, S.D. Antolovich, S.R. Shinde, P.W. Gravett, Influence of coarsened and rafted microstructures on the thermomechanical fatigue of a Ni-base superalloy, Int. J. Fatigue 81 (2015) 191–201.
[41] J. Lapin, T. Pelachova, M. Gebura, The effect of creep exposure on microstructure stability and tensile properties of single crystal nickel based superalloy CMSX-4, Kovove Mater. Met. Mater. 50 (6) (2012) 379–386.
[42] K. An, H.D. Skorpenske, A.D. Stoica, D. Ma, X.L. Wang, E. Cakmak, First in situ lattice strains measurements under load at VULCAN, Metall. Mater. Trans. A 42 (1) (2011) 95–99.
[43] K. Harris, G.L. Erickson, S.L. Sikkenga, W.D. Brentnall, J.M. Aurrecoechea, K.G. Kubarych, Development of two rhenium- containing superalloys for single-crystal blade and directionally solidified vane applications in advanced turbine engines, J. Mater. Eng. Perf. 2 (4) (1993) 481–487.
[44] J. Coakley, D. Dye, Lattice strain evolution in a high volume fraction polycrystal nickel superalloy, Scr. Mater. 67 (5) (2012) 435–438.
[45] H.J. Stone, T.M. Holden, R.C. Reed, On the generation of microstrains during the plastic deformation of Waspaloy, Acta Mater. 47 (17) (1999) 4435–4448.
[46] Q. Liu, J. Coakley, D.N. Seidman, D.C. Dunand, Precipitate Evolution, Creep, Behavior of a W-free Co-based superalloy, Metall. Mater. Trans. A 47 (2016) 6090–6096.
[47] A. Heckl, S. Neumeier, M. Göken, R.F. Singer, The effect of Re and Ru on γ/γ' microstructure, γ-solid solution strengthening and creep strength in nickel-base superalloys, Mater. Sci. Eng. A 528 (2011) 3435–3444.
[48] H.J. Stone, T.M. Holden, R.C. Reed, Determination of the plane specific elastic constants of Waspaloy using neutron diffraction, Scr. Mater. 40 (3) (1999) 353–358.
[49] J. Coakley, E.A. Lass, D. Ma, M. Frost, D.N. Seidman, D.C. Dunand, H.J. Stone, Rafting and elastoplastic deformation of superalloys studied by neutron diffraction, Scr. Mater. 134 (2017) 110–114.
[50] H. Ohtani, M. Yamano, M. Hasebe, Thermodynamic analysis of the Co-Al-C and Ni-Al-C systems by incorporating ab initio energetic calculations into the CALPHAD approach, Calphad 28 (2) (2004) 177–190.
[51] J. Miettinen, Thermodynamic description of the Cu-Al-Ni system at the Cu-Ni side, Calphad 29 (1) (2005) 40–48.
[52] J. Coakley, D. Dye, H. Basoalto, Creep and creep modelling of a multimodal nickel-base superalloy, Acta Mater. 49 (2011) 854–863.
[53] N. Matan, D.C. Cox, P. Carter, M.A. Rist, C.M.F. Rae, R.C. Reed, Creep of CMSX-4 superalloy single crystals: effects of misorientation and temperature, Acta Mater. 47 (5) (1999) 1549–1563.